DOI: 10.1021/cg100253k

CRYSTAL GROWTH & DESIGN Article

2010, Vol. 10
2752–2758

Spectroscopic and Structural Characterization of Two Polymorphs of 1,1,4,4-Tetraphenyl-1,3-butadiene

Alberto Girlando,*[,†] Sandra Ianelli,[†] Ivano Bilotti,[‡] Aldo Brillante,[‡] Raffaele G. Della Valle,[‡] Elisabetta Venuti,[‡] Marcello Campione,[§] Stefano Mora,[§] Leonardo Silvestri,[§] Peter Spearman,[§] and Silvia Tavazzi[§]

[†]*Dipartimento Chimica G.I.A.F., and INSTM-UdR Parma, Parma University, I-43124 Parma, Italy,* [‡]*Dipartimento Chimica Fisica ed Inorganica, and INSTM-UdR Bologna, Bologna University, I-40136 Bologna, Italy, and* [§]*Dipartimento Scienza dei Materiali, Milano-Bicocca University, I-20125 Milano, Italy*

Received February 24, 2010; Revised Manuscript Received April 24, 2010

ABSTRACT: We report a combined spectroscopic and structural study of polymorphism of 1,1,4,4-tetraphenyl-1,3-butadiene (TPB) blue luminescent crystals. We have identified two polymorphs, which can be grown by crystallization of the vapor. The first, α-TPB, has the monoclinic noncentrosymmetric structure ($P2_1$, two molecules per unit cell), whose lattice parameters have already been reported in the literature. The second, β-TPB, is a new polymorph, monoclinic centrosymmetric ($P2_1/c$, four molecules per unit cell). The previously reported triclinic structure, γ-TPB, has not been identified in samples grown by the physical vapor transport method. The effects of the different molecular configuration and packing of α- and β-TPB on Raman scattering, IR, and UV−vis optical properties are discussed.

Introduction

Scientific curiosity and applied science, in particular, materials science, have stimulated growing interest in the polymorphism of molecular crystals.[1] Polymorphs have the same chemical composition but may exhibit different solid-state properties due to the different molecular configuration and/or packing. In the field of organic semiconductors, for instance, a change in the tilting angle of the pentacene molecules within the crystal yields different bandwidths[2] and different carrier-phonon coupling.[3] Different mobilities are therefore expected and have been found experimentally for two polymorphs of a different compound, 5,11-bis(triethylsilylethynyl)anthradithiophene.[4] A further nice example of the effects of molecular packing has been recently reported for the optical properties of three different polymorphs of rubrene.[5]

Single crystal X-ray crystallography is of course the technique of choice for the definitive and direct identification of different polymorphs. However, it is not always applicable in situ, as required for instance for investigating thin films in operating devices, and cannot ascertain phase purity, that is, the coexistence of different polymorphs in the same crystallite. Among other spectroscopic and structural techniques,[1] Raman spectroscopy in the region of lattice vibrations (10−150 cm^{-1}) has recently gained in importance for the identification of different polymorphs and for investigating the phase purity of several organic semiconductors.[6,7] In the present paper, we show how this technique can be fruitfully used, also in connection with other spectroscopic and structural methods, to investigate polymorphism in 1,1,4,4,-tetraphenyl-1,3-butadiene (TPB).

TPB is a well-known highly efficient blue emitting material, and its photoluminescence properties in solution and in polymeric matrices have been investigated both experimentally and theoretically.[8,9] Good emitting properties are preserved in the crystalline state, but very few investigations have been performed on the solid-state properties of this compound. In particular, a triclinic structure has been published in the context of a study of the coordination behavior of TPB,[10] whereas the unit cell parameters of a monoclinic noncentrosymmetric structure have been reported for TPB nanocrystals.[11]

In the course of a study aimed at characterizing the solid-state emitting properties of TPB, we have discovered a new polymorph, which is particularly interesting as it exhibits amplified spontaneous emission (ASE) from the widest crystal face.[12] In the following, we report a detailed structural and spectroscopic study of the new polymorph and of the monoclinic noncentrosymmetric one.[11] We show that the different packing of TPB in the two polymorphs strongly affects the Raman, IR, and UV−vis optical properties. The latter are particularly relevant for device applications. The origin of the optical bands is discussed on the basis of the provided crystallographic data.

Experimental Section

Crystal Growth. TPB was purchased from Sigma-Aldrich and used as received. The single crystals studied in this paper were grown by the physical vapor transport method,[13] by placing TPB powder in a glass crucible at the end of a 75 cm long and 25 mm wide glass-tube. By using a three-zone furnace, the source was heated at 175 °C, whereas the temperature at the middle and the opposite end was 170 and 135 °C, respectively. The nitrogen flux was 50 mL/min. After 15 h, thin tabular crystals of both phases were found fairly uniformly distributed along the growth tube. The thickness of the samples grown in this way is of the order of few micrometers. By increasing the source temperature up to 180 °C, and by increasing the nitrogen flux to 100 mL/min, the thickness of the crystals decreased to a great extent. At the head of the tube the α-phase was predominant. However, the selection of a single polymorph by adjusting the temperature profile along the tube was not accomplished.

Spectroscopic Measurements. The Raman spectra were recorded with a Renishaw System 1000 microspectrometer, and with a Jobin Yvon T64000 triple monochromator Raman microspectrometer.

*To whom correspondence should be addressed. E-mail: girlando@unipr.it.

 Published on Web 05/07/2010

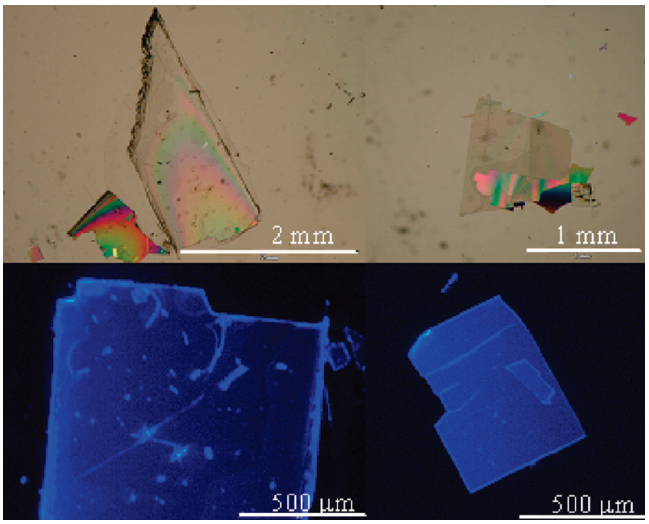

Figure 1. Some examples of TPB crystals grown by the physical vapor transport method. Under the fluorescence microscope (bottom), an intense blue emission is observed.

The former instrument was equipped with an Iridian interference filter to cut the laser line. The exciting lines, from a Kr ion laser, were at 752.5 and 647.1 nm for the two instruments, respectively. The infrared (IR) spectra were obtained with a Bruker IFS-66 FTIR spectrometer, equipped with an A590 microscope. The spectral resolution of the Raman and IR spectra was 2 cm^{-1}. A Perkin-Elmer Lambda 900 spectrometer equipped with Glan-Taylor calcite polarizers to vary the polarization direction of the incoming light was used for the UV−vis spectra.

X-ray Measurements. Intensity data for the two TPB polymorphs were collected at ambient temperature (293 ± 2 K) using graphite monochromated Cu−Kα radiation (λ = 1.54178 Å) on a Siemens AED diffractometer. The structures were solved by direct methods by using the SIR-97 program,[14] and refined by full-matrix least-squares based on F^2 using the SHELX97 program.[15] In the case of the α-polymorph, the number of reflections cuts down by increasing the θ value, so that the ratio reflections/refined parameters is slightly below 8. This is probably due to the poor quality of the crystals.

AFM Measurements. Atomic force microscopy (AFM) measurements were carried out with a Nanoscope V Multi-Mode AFM (Veeco). Surface topography over a micrometric scale was measured in tapping mode with single beam silicon cantilevers with a force constant of 40 N/m and resonance frequency of 250 kHz. Molecular-scale images were collected in contact mode with single beam silicon nitride cantilevers with a force constant of 0.05 N/m. Data processing was performed with the program WSXM.[16]

Results

TPB crystals exhibit different morphologies, platelets, and thicker needles. Some examples of crystals grown by the physical vapor transport method are shown in Figure 1. Under the polarizing microscope one observes different extinction directions in the visible spectral range, sometimes parallel, sometimes oblique with respect to the crystal edges. Of course, both these observations suggest, but do not prove, the existence of different polymorphs. More precise hints come from AFM investigations of the platelets (see below). The platelets are also suited for the UV−vis optical measurements and have been used to demonstrate the occurrence of ASE under laser excitation.[12] On the other hand, platelets are too thin and brittle to allow direct X-ray determination of the structure. It has been recently shown that micro-Raman spectroscopy in the region of the lattice (intermolecular) phonons is a very powerful method to investigate the polymorphism in molecular crystals.[6,7,17,18] In fact, it is sensitive to small structural differences, is nondestructive, can ascertain the phase homogeneity within one sample, and of course can be used equally well on thin or thick samples. We have then adopted this method to disentangle the different TPB phases, and to "bridge" optical, AFM and X-ray measurements.

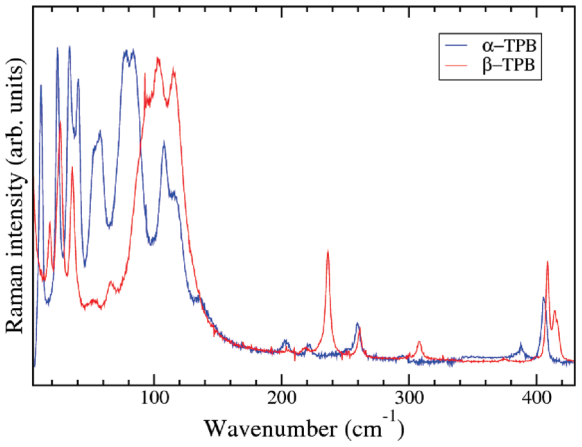

Figure 2. Unpolarized Raman spectra of α- and β-TPB in the low-frequency spectral region. Exciting line: 647.1 nm.

Raman and Infrared Spectra. We have collected Raman spectra on many different crystalline samples, with different morphologies (platelets and needles). We have observed two different types of spectra, clearly associated with two different polymorphs, that we call α- and β-TPB. Notice that the two polymorphs are not associated with crystals of different morphologies; namely, both phases can grow either as platelets or needles. The two different types of spectra are shown in Figure 2, limiting the attention to the most significant spectral region, from 5 to 420 cm^{-1}. The spectra are the superposition of spectra collected with different polarizations of the incoming and scattered light, in order to compensate for intensity differences connected with different polarizations. Figure 2 shows dramatic differences in the lattice phonon spectral region (below ∼180 cm^{-1}). In particular, below 80 cm^{-1} one observes five strong bands for α-TPB, at 11, 24, 33, 41, and 58 cm^{-1}, and three bands for β-TPB, at 18, 26, and 36 cm^{-1}. Furthermore, two groups of bands, unresolved at room temperature, appear in the α-TPB spectrum between 80 and 120 cm^{-1}, whereas only a very broad envelope of several bands is present in the same spectral region for β-TPB. In Figure 2 we notice some spectral differences also above 200 cm^{-1}, namely, in the spectral region of intramolecular vibrations. In particular, there is a clear difference around 400 cm^{-1}, where α-TPB shows one band, and β-TPB two bands. We have observed this difference in all the spectra we have obtained for different samples. Therefore, the region around 400 cm^{-1} can be considered as diagnostic of the two phases as it is the region below 180 cm^{-1}. Other spectral differences between the two phases exist also above 400 cm^{-1}. We do not report nor analyze this spectral region here, deferring to a subsequent paper a more detailed interpretation of the spectra. In any case, and at variance with the other molecular crystals investigated by Raman spectroscopy,[7] spectral differences between the two phases exist not only in the region of the lattice, intermolecular vibrations, but also in the region of intramolecular vibrations. These differences can be certainly ascribed to different molecular conformations within the crystal, a fact not unexpected for a large and flexible molecule as TPB. To confirm that the differences in the high-frequency

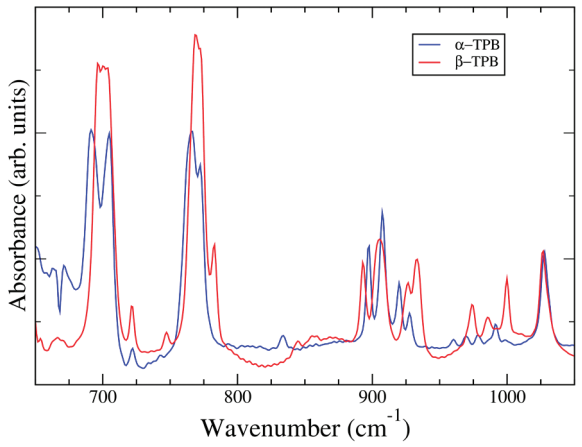

Figure 3. Unpolarized IR spectra of α- and *β*-TPB.

Raman spectra are due to a different molecular conformation within the two polymorphs, we have collected the IR spectra as well, from 600 to 3500 cm^{-1}. We have obtained the absorbance spectra on platelets, with light polarized along the extinction directions observed in the visible region (oblique and parallel to the crystal edges for α- and *β*-TPB, respectively). To make easier the comparison between the two phases, in Figure 3 the unpolarized spectra (average between the two polarizations) are shown, from 650 to 1050 cm^{-1}.

Similar to Raman (Figure 2), there are clear differences between the IR spectra of the two phases, confirming that the molecular conformation is different. As explained before, the analysis of the quite complex vibrational spectra is deferred to a subsequent paper. Here we limit ourselves to state that IR, like Raman, can be used to discriminate between α- and *β*-phases, a quite useful feature in the perspective of looking at very thin films, where Raman may have difficulties due to the weakness of the signal, and in the growth optimization.

X-ray and AFM Measurements. Spectroscopic measurements have allowed us to identify two different TPB polymorphs. As mentioned above, two different crystalline structures have been independently reported for TPB, both with two molecules per cell: a triclinic centrosymmetric ($P\bar{1}$),[10] and a monoclinic noncentrosymmetric ($P2_1$) structure (the latter without atomic coordinates).[11] It was then natural, in a preliminary attempt, to attribute the triclinic structure to α-TPB, with oblique extinctions, and the monoclinic one to *β*-TPB, with parallel extinctions. The X-ray structure determination of two crystalline samples selected on the basis of their Raman spectra showed that this was not the case. The α-polymorph actually corresponds to the monoclinic noncentrosymmetric structure,[11] whereas the structure of the *β*-polymorph is a completely new one, namely, a monoclinic centrosymmetric ($P2_1/c$) structure with four molecules per unit cell. The essential crystallographic parameters of the two structures are reported in Table 1, together with the corresponding data of the triclinic polymorph,[10] that we now name *γ*-TPB. The full crystallographic data of α- and *β*-polymorphs in CIF format are given in the Supporting Information.

Views of the unit cells and of the crystal packings of α- and *β*-polymorphs are reported in Figure 4. The upper part of the figure shows the different molecular packings in the two structures. Both structures are characterized by layers of TPB molecules, with the butadiene skeleton directed along the long crystallographic axis. In *β*-TPB, the butadiene skeletons

Table 1. Essential Crystallographic Data for the α, *β*, and *γ* Polymorphs of TPB

polymorph	α	*β*	*γ*[10]
space group	$P2_1$	$P2_1/c$	$P\bar{1}$
a (Å)	6.259 (2)	9.736 (5)	10.110 (1)
b (Å)	22.164 (4)	8.634 (2)	10.851 (2)
c (Å)	7.362 (3)	24.480 (13)	9.820 (2)
α (deg)	90	90	103.64 (1)
β (deg)	96.349 (4)	97.11 (4)	94.95 (1)
γ (deg)	90	90	99.31 (1)
V (Å^3)	1014.9 (6)	2042.0 (16)	1024.3
Z	2	4	2

are all parallel to the long crystal axis. To obtain a better packing, the molecules are shifted one with respect to the other, in such a way to avoid close contacts between the lateral phenyl groups. On the other hand, in α-TPB the molecules are not parallel but disposed in a sort of herringbone pattern. This patterns actually yields a packing tigther than that of the *β*-phase, with a reduced volume per molecule (Table 1). A more detailed analysis of the crystal packing and of the relative stability of the phases will be performed in a forthcoming paper, following the computational methods we have successfully used for other organic semiconductors.[19] Here we anticipate that the denser α-TPB is indeed more stable than *β*-TPB by about 3 kcal/mol. This difference is likely connected with the different conformation of the TPB molecules in the two polymorphs, already hinted from the Raman and IR spectra.

Figure 5 shows the different TPB conformations within the crystal. In both polymorphs, the TPB molecules occupy general positions, so that there are no symmetry constraints. On the other hand, from Figure 5 one is able to infer the presence of molecular symmetry elements. More detailed analysis shows that indeed in the α polymorph the TPB molecule has approximately C_i symmetry (tolerance of 0.3 Å for the atomic coordinates), and in the *β*-phase it has approximately C_2 symmetry (tolerance 0.6 Å). The difference in the conformation concerns the relative position of the four phenyl groups, the butadiene skeleton being in any case essentially planar. An equilibrium conformation search for the isolated (gas phase) TPB molecule with the MOPAC2009 package[20] shows that both the C_i and C_2 conformation correspond to local minima, with negligible energy difference between the two minima. Interestingly enough, the molecular packing *and* conformation of TPB in the *γ* phase[10] is very similar to that of the *β* phase: the molecules have approximate C_2 symmetry and are arranged with the butadiene skeleton parellel to the long crystallographic axis. Crystal packing and molecular conformation are then strictly connected. Vibrational spectra in the region of intramolecular vibrations will less easily discriminate between the *β* and *γ* polymorphs, as they do between the α and *β* ones.

In parallel with the X-ray crystal structure determination, we have also performed an AFM analysis of the thin platelet used for UV−vis measurements. Figure 6a shows the step-rich surface topography observed over the widest surface of a α-TPB crystal. The majority of steps have a height of 22.0 ± 2.0 Å (see cross-sectional profile in panel b), which is consistent with the length of the *b* axis of this polymorph (22.16 Å), suggesting (010) as the surface exposed by the sample. Nonetheless, as it can be observed in the cross-sectional profile in Figure 6b (red line), some step-edges appear with topographic features indicating the presence of elemental layers with half the previous spacing (i.e., $b/2 = 11.08$ Å). This observation is

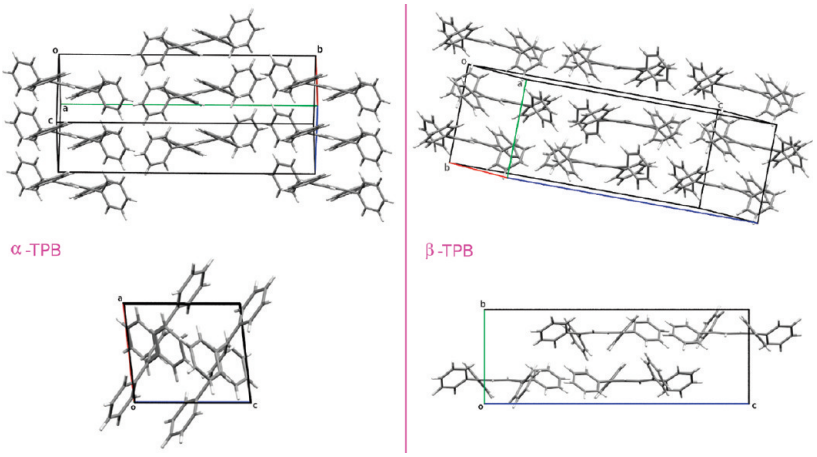

Figure 4. Crystal structure and packing of α-TPB (left) and of *β*-TPB (right). The bottom part of the figure reports the projection of the unit cell on the crystal plane investigated by UV−vis spectroscopy (see below).

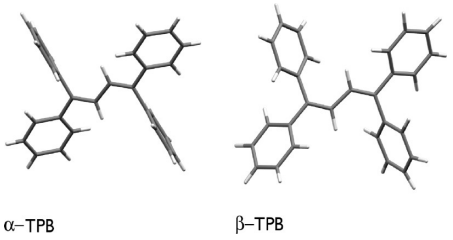

Figure 5. Molecular conformation of TPB in the α and *β* polymorphs.

consistent with the systematic extinction of (0*k*0) X-ray reflections (odd *k*) of the α-TPB polymorph. The assigned orientation of the crystal is substantiated by the molecular-scale analysis of the surface topography of a single terrace reported in Figure 6c. The Fourier analysis of the image contrast (inset) suggests the presence of a rhombic unit-cell in reciprocal space, corresponding in real space to a lattice with parameters 6.2 ± 0.5 Å (short axis), 7.4 ± 0.7 Å (long axis), and enclosed angle 91 ± 3° (Figure 6d). These parameters are consistent with the *a*, *c*, and *β* parameters deduced by X-ray (6.259 Å, 7.362 Å, 96.349°, see Figure 5).

The topography of the widest surface of a *β*-TPB crystal, as imaged by AFM, is reported in Figure 7a. The surface is characterized by the presence of several growth steps separated by molecularly flat terraces with an average width of 500 nm. As shown by the cross-sectional profile in Figure 7b, the steps are uniform in height, indicating a spacing among molecular layers of 9.8 ± 0.7 Å. This spacing is consistent with that corresponding to (100) planes (9.66 Å), as deduced by X-ray measurements. The assignment of (100) as the exposed crystal surface is corroborated by a molecular-scale analysis of the surface topography. Figure 7c shows the surface corrugation as measured by AFM over a molecularly flat terrace. In the 2D Fourier-transform of the image contrast (inset), enhanced intensities form a rectangular reciprocal lattice, which corresponds to the real-space corrugation reported in Figure 7d. The extracted unit cell parameters are 9.3 ± 0.6 Å (short axis), 26.6 ± 1.8 Å (long axis), and enclosed angle 89.1 ± 1.4°. These parameters are consistent with the *b*, *c*, and α parameters deduced by X-ray (8.634 Å, 24.480 Å, 90°; see Table 1).

UV−Vis Spectra. Having fully clarified the crystal structures and face orientation of the two TPB polymorphs, we are now in the position to interpret the UV−vis absorption spectra of TPB, of paramount importance for the assessment of the optical properties of TPB crystals and for the full exploitation in emitting devices.[12] The polarized absorption spectra of the exposed *ac* and *bc* crystal faces of α- and *β*-TPB, respectively, are reported in Figure 8.

In order to interpret the spectra, we have calculated the electronic optical transitions of the isolated TPB molecule in a vacuum with the Gaussian03 program,[21] by adopting the time-dependent density functional method (TD-DFT). The 10 lowest energy molecular singlet transitions have been calculated by employing the hybrid functional B3LYP with the 6-31G(d,p) basis set, and by using the molecular geometries given by the crystallographic data of the two polymorphs. The lowest energy electronic transition is found at 3.62 eV for TPB with the (approximate) C_i conformation of the α polymorph, and at 3.56 eV for the C_2 conformation of the *β* polymorph (Figure 5), followed by molecular transitions at higher energies. In both cases, the lowest transition is by far the strongest transition calculated in the interval 3−4.8 eV, and is strongly polarized along the longest inertial axis of the molecule (L), that is, along the butadiene skeleton, where the HOMO and LUMO are mostly localized. All the components of the transition dipole moment in the orthogonal molecular coordinate system L, M, N (where M and N are the shortest inertial axes, N being normal to the butadiene skeleton) are reported in Table 2.

The α-TPB polymorph has two molecules per unit cell, so that each molecular electronic transition gives rise to two excitonic bands. Both bands are optically allowed at $\mathbf{k} = 0$ (center of the Brillouin zone), and they are polarized in the *ac* plane and along the monoclinic *b* axis, respectively. The projections along the *a*, *b*, *c** axes of the electronic molecular transition dipole moments at about 3.6 eV are reported in Table 2, together with the projections of the corresponding unit cell excitonic transition dipole moments at $\mathbf{k} = 0$. The two excitonic transition dipole moments in the *abc** frame of reference are {7.39, 0, 4.54} Debye and {0, 8.19, 0} Debye, respectively. The *a* and *c** axes of the frame of reference are in the exposed crystalline face, as deduced from AFM (see above), while the *b* axis is along the normal to the surface. The two excitonic transitions have comparable intensities, and the direction of polarization of the *ac* component is predicted at 32° to the *a* axis.

Figure 8a shows the measured absorption spectra taken on the accessible *ac* face of α-TPB crystal. The two continuous

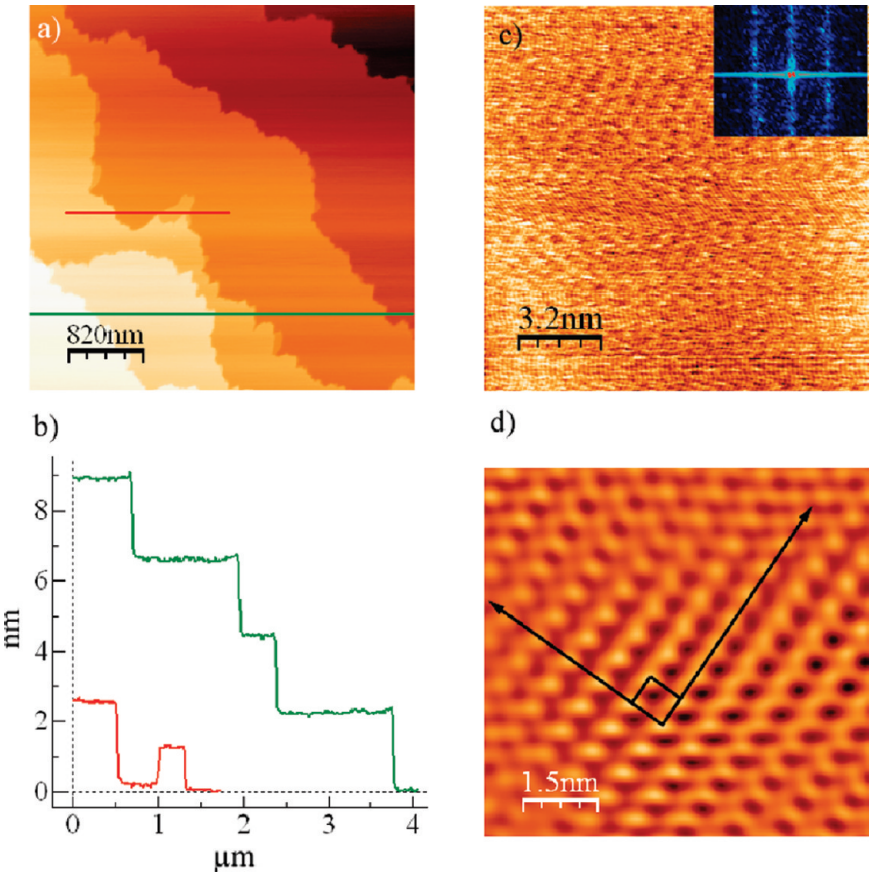

Figure 6. (a) AFM surface morphology of one α-TPB crystal; (b) cross-sectional profile showing steps with spacing 22.0 ± 2.0 Å (green line) and other features with half spacing (red line). (c) Molecular-scale AFM image taken over a single terrace of the surface in (a); inset: 2D Fourier transform of the image contrast. (d) Fourier filtered image with indication of unit cell axes.

curves correspond to two orthogonal polarizations giving the maximum (∥) and minimum (⊥) absorbance at normal incidence between 3 and 4 eV. The ∥ spectrum saturates above ~3 eV, in correspondence with the strong excitation calculated at 3.6 eV. Despite the saturation, a band can be recognized. This band is negligible in the ⊥ spectrum, as expected. The maximum absorption at normal incidence is typically measured when the electric field of the incident light forms an angle of about 30° to one of the edges of the crystal. The comparison with the predicted value of 32° indicates that this edge corresponds to the *a* axis and the intense saturated band is attributed to the *ac* excitonic state of α-TPB. Figure 8a spectra also show that a second peak appears at 4.45 eV. This peak is peculiar to the α polymorph and is attributable to a weaker molecular excitation at higher energy. In that energy range TD-DFT calculations indeed predict a molecular transition with a non-negligible dipole component along the direction of minimum absorption in the crystal.

To probe the transitions with components along the *b* axis normal to the surface, we have performed oblique incidence measurements using light polarized in the plane of incidence, the latter being defined as the plane formed by the direction of polarization of minimum absorption at normal incidence and the normal to the surface. A definite band emerges centered at about 3.77 eV, corresponding to the *b* polarized excitonic transition.

In *β*-TPB there are four molecules per unit cell, so that each molecular electronic transition gives rise to four excitonic bands. Only two of them are optically allowed, and they are polarized in the *ac* plane and along the monoclinic *b* axis, respectively. For the molecular transition at lowest energy, the two allowed excitonic transition dipole moments in the *bca** frame of reference are {0, 16.44, 1.36} Debye and {0.50, 0, 0} Debye, respectively (Table 2). The *b* and *c* axes of the reference frame are in the exposed face, as deduced from AFM, while the *a** axis is along the normal to the surface. From Table 2 one predicts that the *b* component of the lowest energy molecular transition is negligible with respect to the *ac* component, the latter being mostly polarized along *c*.

Figure 8b shows the measured absorption spectra taken on the accessible *bc* face of *β*-TPB crystal. The two continuous curves correspond to two orthogonal polarizations giving the minimum (⊥) and maximum (∥) absorbance between 3.0 and 4.5 eV. The latter spectrum clearly saturates, in correspondence with a strong polarized band with absorption edge at about 3 eV. This band disappears in the ⊥ spectrum taken at normal incidence; it is also negligible in the spectra taken at oblique incidence (20 and 50° in Figure 8b). For the oblique incidence spectra, the light is polarized in the plane of incidence, defined by the normal to the surface and the direction of minimum absorption found at normal incidence. Thus, the band with edge at about 3.0 eV dominates the spectrum and is strongly polarized along the *c* axis. From Table 2 predictions one easily attributes the band to the *ac* excitonic component, strongly polarized in the *bc* accessible face. As far as the higher energy molecular transitions are concerned, no peak is observed in correspondence with the band at about 4.5 eV detected in the α polymorph. Indeed, TD-DFT calculations show that the relevant transition dipole moment has a different orientation in the *β* polymorph, such

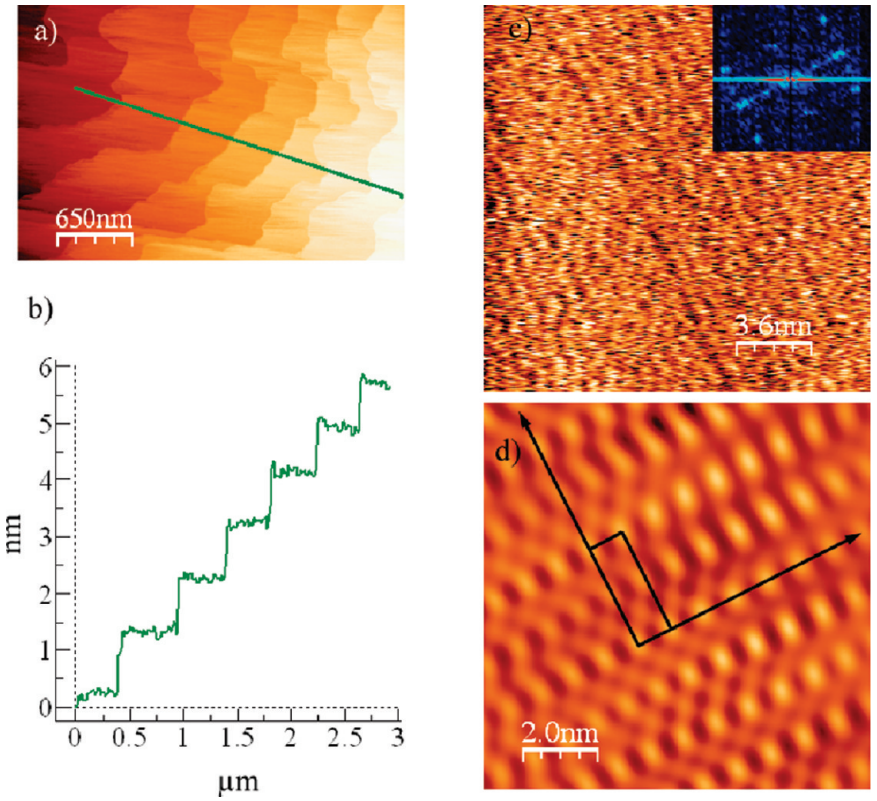

Figure 7. (a) AFM surface morphology of a β-TPB crystal; (b) cross-sectional profile taken along the green line showing elemental steps with spacing 9.8 ± 0.7 Å; (c) molecular-scale AFM image taken over a single terrace of the surface in (a); inset: 2D Fourier transform of the image contrast; (d) Fourier-filtered image with indication of unit cell axes.

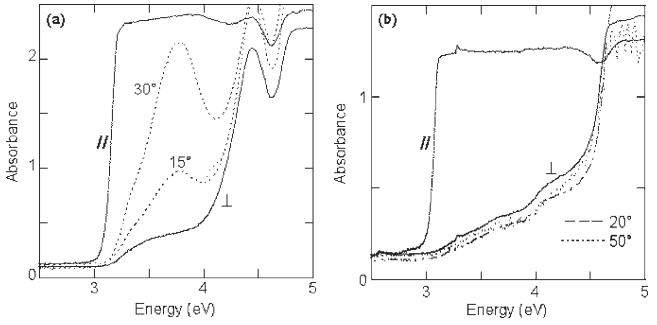

Figure 8. Polarized absorption spectra of (a) α-TPB (*ac* crystal face) and (b) β-TPB (*bc* crystal face). The ∥ and ⊥ symbols relevant to the continuous lines indicate the two orthogonal polarizations corresponding to the maximum and minimum absorption for normal incidence. The dashed lines indicate spectra taken at oblique incidence (see text).

Table 2. Calculated Dipole Moments (in Debye) of the Lowest Energy Molecular Transition of TPB in the α- and β-Phases, Referred to the Molecular L, M, N Axes, and Projected along the Orthogonalized Crystal Axes[a]

	α-TPB			β-TPB		
	L	M	N	L	M	N
molecular axes	−8.43	0.26	0.02	−8.22	0.73	0.12
crystal axes	*a*	*b*	*c**	*b*	*c*	*a**
molecule 1	5.23	5.79	3.21	−0.25	−8.22	0.68
molecule 2	−5.23	5.79	−3.21	0.25	8.22	−0.68
molecule 3				−0.25	8.22	−0.68
molecule 4				0.25	−8.22	0.68
excitonic transitions						
ac	7.39	0	4.54	0	16.44	1.36
b	0	8.19	0	0.50	0	0

[a] The corresponding unit cell exciton dipole moments (in Debye) are also reported.

that it would be observable only for very large angles of incidence, not experimentally accessible on our samples.

Discussion and Conclusions

From the present experiments, it turns out that TPB can grow in at least three polymorphic forms. Of these, the α phase is the most frequently encountered and is the thermodynamically stable phase at ambient conditions. Small quantities β-TPB crystals can be found in batches grown by the vapor transport method. We have started to explore other methods of crystal growth and verified that the β polymorph occurs more often in crystals grown from the melted material. However, we still have to find the appropriate conditions to grow one or the other polymorph. Preliminary investigations by Raman have shown that a third polymorph, that we tentatively associate to the γ-phase,[10] occurs in crystalline agglomerates obtained by fast recrystallization from *n*-pentane.

TPB has mobile pendant phenyl rings, and it is not surprising that different polymorphs present different molecular conformations. This fact makes it easier to discriminate the α from the β polymorph, since one can use conventional vibrational spectroscopy in the region of intramolecular modes. On the other hand, the analysis and interpretation of the spectra in this spectral region is more difficult and is deferred to a forthcoming paper.

As mentioned in the Introduction, studying the polymorphism is of utmost importance in molecular materials, as the

physical properties of interest may differ from one polymorph to the other.[2] From this point of view, TPB can be considered a further significant example. TPB is indeed being studied for its UV−vis optical properties, and these are remarkably different in α- and β-TPB, as shown in the previous section. We stress however that these differences are not related to the different molecular conformation of TPB in the two polymorphs. The conformational change involves the phenyl groups, whereas the electronic transition of interest mostly involves the butadiene skeleton, which remains essentially planar. The transition dipole moments of the isolated molecules are indeed similar, 8.43 and 8.25 D, for the C_i and C_2 conformations, respectively. What is important is the relative orientation of the molecules within the crystal and with respect to the most developed crystal face.

The bottom part of Figure 4 shows the orientation of TPB molecules in the unit cell and with respect to the *ac* and *bc* crystal faces used for the UV−vis measurements. It is seen that in the α phase the butadiene backbones are not parallel to each other, being arranged in a sort of herringbone structure. In addition, they are not parallel to the most developed *ac* crystal face. On the other hand, in the β-phase the butadiene skeletons are parallel to each other, and parallel to the *c* axis, which also corresponds to the extinction direction. As a result, one excitonic state dominates the UV−vis absorption spectrum of β-TPB and the intensity of the transition (proportional to the squared transition dipole moment per unit volume) along the corresponding direction of polarization is about two times larger in the β than in the α polymorph (Table 2).

Work is in progress in our laboratories to develop an appropriate protocol for the growth of the β polymorph. In this process, we are assisted by the spectroscopic identification tools presented in this paper. Furthermore, analysis of the factors which determine the molecular packing within the crystal will also allow one to use substituents different from the phenyl group to engineer favorable arrangements of the butadiene skeleton within the crystal.[22] Considering that different substituents also are able to shift the maximum of luminescence toward the visible region,[23] one can appropriately use molecular *and* crystal engineering to obtain optimum luminescence in the spectral region of interest.

Acknowledgment. The Milano-Bicocca group thanks the Cariplo Foundation for financial support.

Supporting Information Available: X-ray crystallographic data in CIF format (these data also have been submitted to the Cambridge Crystallographic Database). This material is available free of charge via the Internet at http://pubs.acs.org/.

References

(1) Bernstein, J. *Polymorphism in Molecular Crystals*; Oxford University Press: New York, NY, 2002.
(2) (a) Haddon, R. C.; Chi, X.; Itkis, M. E.; Antony, J. E.; Eaton, D. L.; Siegrist, T.; Mattheus, C. C.; Palstra, T. T. M. *J. Phys. Chem. B* **2002**, *106*, 8288. (b) Troisi, A.; Orlandi, G.; Anthony, J. E. *Chem. Mater.* **2005**, *17*, 5024. (c) Yoshida, H.; Sato, N. *Phys. Reb. B* **2008**, *77*, 235205.
(3) Della Valle, R. G.; Brillante, A.; Farina, L.; Venuti, E.; Masino, M.; Girlando, A. *Mol. Cryst. Liq. Cryst.* **2004**, *416*, 145.
(4) Jurchescu, O. D.; Mourey, D. A.; Subramanian, S.; Parkin, S. R.; Vogel, B. M.; Anthony, J. E.; Jackson, T. N.; Gundlach, D. *J. Phys. Rev. B* **2009**, *80*, 085201.
(5) Huang, L.; Liao, Q.; Shi, Q.; Fu, H.; Ma, J.; Yao, J. *J. Mater. Chem.* **2010**, *20*, 159.
(6) Brillante, A.; Bilotti, I; Della Valle, R. G.; Venuti, E.; Masino, M.; Girlando, A. *Adv. Mater.* **2005**, *17*, 2549.
(7) Brillante, A.; Bilotti, I; Della Valle, R. G.; Venuti, E.; Girlando, A. *CrystEngComm* **2008**, *10*, 937.
(8) Wallace-Williams, S. E.; Schwartz, B. J.; Møller, S.; Goldbeck, R. A.; Yee, W. A.; El-Bayoumi, M. A.; Kliger, D. S. *J. Phys. Chem.* **1994**, *98*, 60.
(9) (a) Lee, M.; Haseltine, J. N.; Smith, A. B., III; Hochstrasser, R. M. *J. Amer. Chem. soc.* **1989**, *111*, 5044. (b) Ponder, M; Mathies, R. *J. Phys. Chem.* **1983**, *87*, 5090. (c) Huang, J.; Bekiari, V.; Lianos, P.; Couris, S. *J. Lumin.* **1999**, *81*, 285. (d) Kido, J.; Shinoya, H.; Nagai, K. *Appl. Phys. Lett.* **1995**, *67*, 2281. (e) Peng, Q.; Yi, Y.; Shuai, Z.; Shao, J. *J. Amer. Chem. Soc.* **2007**, *129*, 9333.
(10) Ino, I.; Wu, L. P.; Munakata, M.; Kuroda-Sowa, T.; Maekawa, M.; Suenaga, Y.; Sakai, R. *Inorg. Chem.* **2000**, *39*, 5430.
(11) Baba, K.; Kasai, H.; Okada, S.; Oikawa, H.; Nakanishi, H. *Opt. Mater.* **2002**, *21*, 591.
(12) Tavazzi, S.; Silvestri, L.; Miozzo, L.; Papagni, A.; Spearman, P.; Ianelli, S.; Girlando, A.; Camposeo, A.; Polo, M.; Pisignano, D. *ChemPhysChem* **2010**, *11*, 429.
(13) Laudise, R. A.; Kloc, Ch.; Simpkins, P. G.; Siegrist, T. *J. Cryst. Growth* **1998**, *187*, 449.
(14) Altomare, A.; Burla, M. C.; Camalli, M.; Cascarano, G.; Giacovazzo, C.; Guagliardi, A.; Moliterni, A. G. G.; Polidori, G.; Spagna, R. *J. Appl. Crystallogr.* **1999**, *32*, 115.
(15) Sheldrick, G. M. *Acta Crystallogr.* **2008**, *A64*, 112.
(16) Horcas, I.; Fernández, R.; Gómez-Rodríguez, J. M.; Colchero, J.; Gómez-Herrero, J.; Baro, A. M. *Rev. Sci. Instrum.* **2007**, *78*, 013705.
(17) Brillante, A.; Della Valle, R. G.; Farina, L.; Girlando, A.; Masino, M.; Venuti, E. *Chem. Phys. Lett.* **2002**, *357*, 32.
(18) Brillante, A.; Bilotti, I.; Della Valle, R. G.; Venuti, E.; Milita, S.; Dionigi, C.; Borgatti, F.; Lazar, A. N.; Biscarini, F.; Mas-Torrent, M.; Oxtoby, N. S.; Crivillers, N.; Veciana, J.; Rovira, C.; Leufgen, M.; Schmidt, G.; Molenkamp, L. W. *CrystEngComm* **2008**, *10*, 1899.
(19) Venuti, E.; Della Valle, R. G.; Brillante, A.; Masino, M.; Girlando, A. *J. Am. Chem. Soc.* **2002**, *124*, 2128.
(20) Stewart, J. J. P. *J. Mol. Modeling* **2007**, *13*, 1173 http://www.openmopac.net.
(21) Frisch, M. J; Trucks, G. W.; Schlegel, H. B.; Scuseria, G. E.; Robb, M. A.; Cheeseman, J. R.; Montgomery, J. A., Jr.; Vreven, T.; Kudin, K. N.; Burant, J. C.; Millam, J. M.; Iyengar, S. S.; Tomasi, J.; Barone, V.; Mennucci, B.; Cossi, M.; Scalmani, G.; Rega, N.; Petersson, G. A.; Nakatsuji, H.; Hada, M.; Ehara, M.; Toyota, K.; Fukuda, R.; Hasegawa, J.; Ishida, M.; Nakajima, T.; Honda, Y.; Kitao, O.; Nakai, H.; Klene, M.; Li, X.; Knox, J. E.; Hratchian, H. P.; Cross, J. B.; Bakken, V.; Adamo, C.; Jaramillo, J.; Gomperts, R.; Stratmann, R. E.; Yazyev, O.; Austin, A. J.; Cammi, R.; Pomelli, C.; Ochterski, J. W.; Ayala, P. Y.; Morokuma, K.; Voth, G. A.; Salvador, P.; Dannenberg, J. J.; Zakrzewski, V. G.; Dapprich, S.; Daniels, A. D.; Strain, M. C.; Farkas, O.; Malick, D. K.; Rabuck, A. D.; Raghavachari, K.; Foresman, J. B.; Ortiz, J. V.; Cui, Q.; Baboul, A. G.; Clifford, S.; Cioslowski, J.; Stefanov, B. B.; Liu, G.; Liashenko, A.; Piskorz, P.; Komaromi, I.; Martin, R. L.; Fox, D. J.; Keith, T.; Al-Laham, M. A.; Peng, C. Y.; Nanayakkara, A.; Challacombe, M.; Gill, P. M. W.; Johnson, B.; Chen, W.; Wong, M. W.; Gonzalez, C.; Pople, J. A. *Gaussian03*, revision D.02; Gaussian Inc.: Wallingford, CT, 2004.
(22) Anthony, J. E.; Eaton, D. L.; Parkin, S. R. *Org. Lett.* **2002**, *4*, 15.
(23) Itami, K.; Ushiogi, Y.; Nokami, T.; Ohashi, Y.; Yoshida, J. *Org. Lett.* **2004**, *6*, 3695.